and highly strained states, respectively. By applying a site simulation based on a ligand-field model, XMCD spectra at Fe $L_{2,3}$ edges for these three samples (Fig. 2(a)) exhibit two negative signals and one positive signal, which correspond to Fe^{2+} and Fe^{3+} cations at octahedral (O_h) sites, and Fe^{3+} cations at tetrahedral (T_d) sites, respectively. In addition, the sample with a SRO matrix exhibits a decreased intensity of signal in Fe^{3+} T_d sites and an increased intensity in Fe^{3+} O_h sites relative to the other two samples, revealing that more Fe^{3+} cations prefer to occupy the O_h sites in this case. In contrast, XMCD spectra measured at Co $L_{2,3}$ edges (Fig. 2(b)) show a significant discrepancy among these three samples. Although Co XMCD measured from the samples with BFO and STO matrices showed the same line shape and were consistent with the reference XMCD of Co^{2+} at O_h sites, the BFO matrix possessed a much larger XMCD signal than the other two. The simulation of the XMCD spectrum measured from the sample with a SRO matrix reveals a mixture of Co^{2+} cations at T_d and O_h sites. The existence of Fe^{2+} O_h sites and Co^{2+} T_d sites indicates that site exchange occurs in these systems because a strain effect or oxygen vacancies can readily break the symmetry and redistribute cations and charges. Based on the results of site simulation, the ratio of Fe^{3+} T_d sites and O_h sites was obtained as ~ 0.78 for nearly strain-free CFO, ~ 0.84 for moderately strained CFO and ~ 0.56 for highly strained CFO. The Co^{2+} cations occupy solely the O_h sites for nearly strain-free and moderately strained cases, which retain similar electronic structures near those of the CFO references. The highly strained CFO has a ratio of Co^{2+} T_d sites and O_h site near one.

The work of this team delivers new concepts to design functional core-shell mesocrystals and stress-mediated functionalities of mesocrystals. The results from XAS-XMCD were a key to reveal the insight of these studies. (Reported by Ying-Hao Chu)

This report features the work of Ying-Hao Chu and his co-workers published in Small ***33,*** *4117 (2015) and Sci. Rep.* ***5,*** *12073 (2015).*

References

1. S. C. Liao, Y. L. Chen, W. C. Kuo, J. Cheung, W. C. Wang, X. Cheng, Y. Y. Chin, Y. Z. Chen, H. J. Liu, H. J. Lin, C. T. Chen, J. Y. Juang, Y. L. Chueh, N. Valanoor, Y. H. Chu, and C. H. Lai, Small **11**, 4117 (2015).
2. H. J. Liu, Y. Y. Liu, C. Y. Tsai, S. C. Liao, Y. J. Chen, H. J. Lin, W. F. Hsieh, C. H. Lai, J. Y. Li, C. T. Chen, Q. He, and Y. H. Chu, Sci. Rep. **5**, 12073 (2015).

Itinerant Hole Carriers Mediate Local Magnetic Moments

Diluted magnetic semiconductors (DMS) have received much attention due to the possibility of utilizing both charge and spin degrees of freedom in electronic devices.[1,2] To realize functional spintronic devices, it is important to have full control of the carrier density and ferromagnetic Curie temperature (T_C). A newly found DMS, $Ba_{1-x}K_x(Zn_{1-y}Mn_y)_2As_2$ (Mn-$BaZn_2As_2$),[3] is isostructural with iron-based superconductors[4] of type "122" and has a T_C up to 230 K.[5] This material has an advantage that the charge-reservoir Ba layer and the ferromagnetic ZnAs layer are spatially separated, as shown in Fig. 1, which independently allows control of the amount of hole carriers by K substitution into the Ba layer and that of magnetic elements on substituting Mn into the ZnAs layer. As DMS in this series show great possibilities for next-generation spintronic devices, Suzuki *et al.*[6] investigated the electronic and magnetic structures of Mn-$BaZn_2As_2$ and compared them with archetypal Mn-doped DMS materials such as $Ga_{1-x}Mn_xAs$.

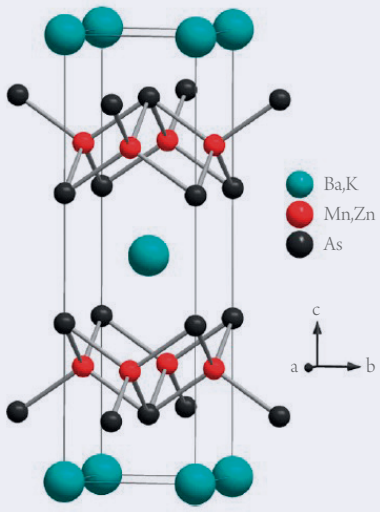

Fig. 1: Crystal structure of Mn-$BaZn_2As_2$ (structure of type $ThCr_2Si_2$, space group *I4/mmm*). [Reproduced from Ref. 4]

They recorded X-ray absorption spectroscopy (XAS) and resonant photoemission spectroscopy (RPES) of $Ba_{0.7}K_{0.3}(Zn_{0.85}Mn_{0.15})_2As_2$ (Mn-$BaZn_2As_2$) polycrystalline samples at **BL11A1** of the TLS and at BL-2C of Photon Factory, respectively. The samples were filed *in situ* before the measurements to ensure fresh surfaces.

Figure 2 shows the Mn $L_{2,3}$-edge XAS of Mn-$BaZn_2As_2$ compared with those of reference Mn materials. The energy of the main Mn L_3-edge XAS signal shows the valence of the Mn atom. The main Mn L_3-edge XAS signal of Mn-$BaZn_2As_2$ is located above that of Mn metal, below that of $LaMnO_3$ (Mn^{3+}), and the same as of Mn^{2+} compounds; this result shows the Mn atom in Mn-$BaZn_2As_2$ to take valence 2+. The Mn line shape of the $L_{2,3}$-edge XAS reflects the localized nature of Mn *3d* states; as the multiplet structures become clearer, the Mn *3d* electronic structures become more localized. The XAS line shape of Mn-$BaZn_2As_2$ is intermediate between those of two DMS systems, $Ga_{0.922}Mn_{0.078}As$ (GaMnAs) and $Ga_{0.958}Mn_{0.042}N$ (GaMnN). The shoulder structures at 640 and 643 eV are more pronounced than in GaMnAs and weaker than in GaMnN. This effect indicates that Mn *3d* orbitals strongly hybridize with the surrounding As *4p* orbitals as in GaMnAs and GaMnN; the strength of hybridization is greater than in GaMnAs but weaker than in GaMnN.

To extract the local electronic structures of the doped Mn, they performed RPES experiments using photon energies at the Mn L_3-edge. The *3d* partial density of states (PDOS) of a transition metal in solids was deduced on taking the difference of valence-band photoemission spectra between on-resonant and off-resonant photon energies. For Mn-$BaZn_2As_2$, on-resonant and off-resonant photon energies at Mn L_3-edge are estimated to be 635 and 638.5 eV from Mn L_3-edge XAS, shown in Fig. 3(a). By subtracting the off-resonant spectra from the on-resonant spectra, they deduced the PDOS of Mn *3d* orbitals as shown in Fig. 3(b). The DOS is small at E_F, finite between -2 eV and E_F, and has a maximum at -4 eV. The deduced Mn *3d* PDOS is compared with that of $Ga_{0.957}Mn_{0.043}As$[7] in Fig. 3(c); the overall spectral shapes are similar. This result indicates that the electronic states of doped Mn are alike in these two DMS systems; the similarity originates from the same chemical valence 2+ of the Mn atoms and the tetrahedral coordination with the As *4p* orbitals. Holes are thus predominantly introduced into the valence band composed mainly of As *4p* states; the local magnetic moments with $S = 5/2$ are formed there in the presence of Hund's coupling between electrons of the d^5 configuration.

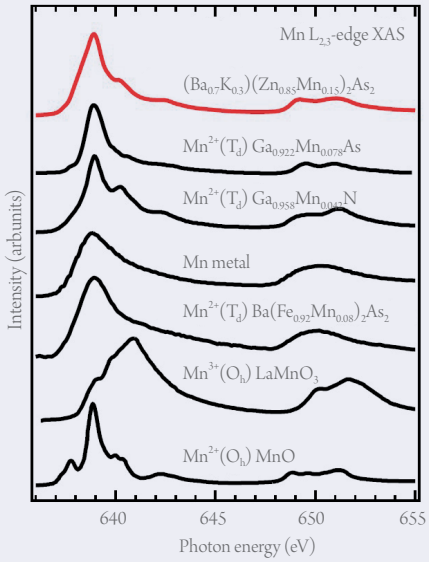

Fig. 2: Mn $L_{2,3}$-edge XAS of Mn-$BaZn_2As_2$, compared with those of $Ga_{0.922}Mn_{0.078}As$, $Ga_{0.958}Mn_{0.042}N$, Mn metal, $Ba(Fe_{0.92}Mn_{0.08})_2As_2$, $LaMnO_3$, and MnO. The valence and local symmetry of Mn atoms are indicated for each compound. [Reproduced from Ref. 6]

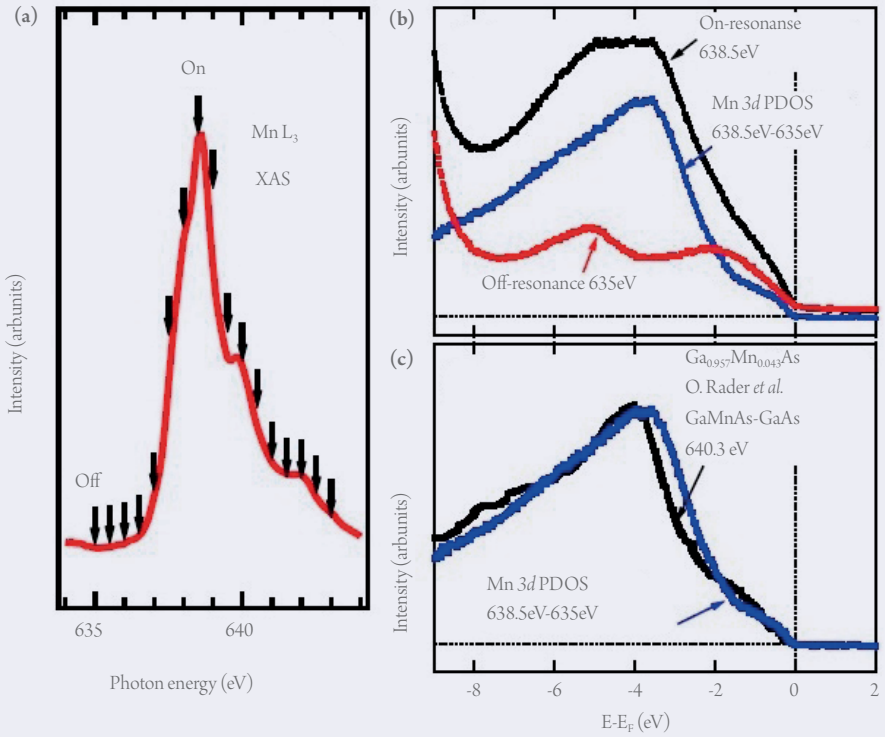

Fig. 3: (a) On- and off-resonance photon energies are shown with arrows on Mn L_3-edge XAS of Mn-$BaZn_2As_2$. (b) Mn 3*d* PDOS deduced on subtracting the off-resonance spectrum ($h\nu = 635$ eV) from the on-resonance spectrum ($h\nu = 638.5$ eV). (c) Mn 3*d* PDOS of $Ga_{0.957}Mn_{0.043}As$ (Ref. 7) compared with that of Mn-$BaZn_2As_2$. [Reproduced from Ref. 6]

Suzuki *et al.* studied the electronic structures of $Ba_{1-x}K_x(Zn_{1-y}Mn_y)_2As_2$ related to Mn 3*d* states using XAS and RPES measurements. The Mn $L_{2,3}$-edge XAS indicate that the doped Mn atoms have a valence 2+ and are strongly hybridized with the As 4*p* orbitals, as in archetypical DMS GaMnAs. The Mn 3*d* PDOS obtained from RPES leads to the d^5 electronic configurations of Mn atoms with local magnetic moment $S = 5/2$. They concluded that the doped holes go into the top of the As 4*p*-derived valence band and are weakly bound to the Mn local spins. The ferromagnetic correlation between the local spins mediated by the hole carriers induces ferromagnetism in Mn-$BaZn_2As_2$. (Reported by Jun Okamoto)

This report features the work of Hakuto Suzuki, Atsushi Fujimori and their co-workers published in Phys. Rev. B ***95****, 140401(R) (2015).*

References

1. H. Ohno, Science **281**, 951 (1998).
2. T. Dietl, Nature Mater. **9**, 965 (2010).
3. K. Zhao, Z. Deng, X. C. Wang, W. Han, J. L. Zhu, X. Li, Q. Q. Liu, R. C. Yu, T. Goko, B. Frandsen, L. Liu, F. Ning, Y. J. Uemura, H. Dabkowska, G. M. Luke, H. Luetkens, E. Morenzoni, S. R. Dunsiger, A. Senyshyn, P. Bni, and C. Q. Jin, Nature Commun. **4**, 1442 (2013).
4. M. Rotter, M. Tegel, and D. Johrendt, Phys. Rev. Lett. **101**, 107006 (2008).
5. K. Zhao, B. Chen, G. Zhao, Z. Yuan, Q. Liu, Z. Deng, J. Zhu, and C. Jin, Chin. Sci. Bull. **59**, 2524 (2014).
6. H. Suzuki, K. Zhao, G. Shibata, Y. Takahashi, S. Sakamoto, K. Yoshimatsu, B. J. Chen, H. Kumigashira, F.-H. Chang, H.-J. Lin, D. J. Huang, C. T. Chen, B. Gu, S. Maekawa, Y. J. Uemura, C. Q. Jin, and A. Fujimori, Phys. Rev. B **91**, 140401(R) (2015).
7. O. Rader, C. Pampuch, A. M. Shikin, W. Gudat, J. Okabayashi, T. Mizokawa, A. Fujimori, T. Hayashi, M. Tanaka, A. Tanaka, and A. Kimura, Phys. Rev. B **69**, 075202 (2004).

New Features of Topological Insulators from Terahertz Emission Spectroscopy

Topological insulators (TI) are a fascinating form of quantum matter that possesses a Dirac cone-like conducting surface state on its surfaces. The surface state exhibits novel properties, such as time-reversal protection against back- scattering and spin-polarized current. TI were predicted to have a high potential in applications of quantum computation. From the point of view of experimental study of TI, two key issues are how to determine the surface state and what characteristic properties the Dirac fermions possess. Several experimental techniques, such as angle-resolved photoemission spectroscopy (ARPES) and scanning tunneling microscopy, have been applied to gain insights on these issues.

For example, an unoccupied second surface state (second SS) and bulk bands (BB) located above the first SS by 1.5 eV have been observed in Bi_2Se_3 with the two-photon photoemission spectroscopy of ARPES measurements.[1] These second SS and BB play important roles in TI's optical coupling and related optoelectronic applications. Earlier studies on TI with optical spectroscopy, such as second harmonic generation and pump-probe measurements,[2,3] did not clearly identify the influences of these second SS and BB. This is because, during the optical excitation there are numerous phenomena occur simultaneously, such as photo-electron emission, nonlinear light conversion and generation of hot photo-carriers. Recently, it was proposed that terahertz (THz) emission was suggested to be a potential candidate capable of examining not only nonlinear light conversion but also transient dynamics of photo-excited carriers. In the THz and mid-infrared spectral ranges, electric-field-resolved light is a practical approach, which yields abundant information from the materials because of the available phase information of the light.

Chien-Ming Tu and his co-workers measured the THz emission spectra of TI samples with varied doping.[4] Figure 1(a) shows the schematics of their experiments. P-polarized 75-fs optical pump pulses, at wavelength 800 nm, illuminated the (111) surfaces of TI crystals at incident angle 45° to generate THz radiation; the emitted THz waveform